TU Delft

Delft University of Technology

Beamforming for a Fast Scanning Phased Array Weather Radar

Dash, Tworit; Gîrdianu, Alexandru; Krasnov, Oleg A.; Yarovoy, Alexander

DOI
10.23919/EuRAD58043.2023.10289351

Publication date
2023

Document Version
Final published version

Published in
Proceedings of the 2023 20th European Radar Conference (EuRAD)

Citation (APA)
Dash, T., Gîrdianu, A., Krasnov, O. A., & Yarovoy, A. (2023). Beamforming for a Fast Scanning Phased Array Weather Radar. In *Proceedings of the 2023 20th European Radar Conference (EuRAD)* (pp. 290-293). IEEE. https://doi.org/10.23919/EuRAD58043.2023.10289351

Important note
To cite this publication, please use the final published version (if applicable).
Please check the document version above.

Copyright
Other than for strictly personal use, it is not permitted to download, forward or distribute the text or part of it, without the consent of the author(s) and/or copyright holder(s), unless the work is under an open content license such as Creative Commons.

Takedown policy
Please contact us and provide details if you believe this document breaches copyrights.
We will remove access to the work immediately and investigate your claim.

This work is downloaded from Delft University of Technology.
For technical reasons the number of authors shown on this cover page is limited to a maximum of 10.

Green Open Access added to TU Delft Institutional Repository

'You share, we take care!' - Taverne project

https://www.openaccess.nl/en/you-share-we-take-care

Otherwise as indicated in the copyright section: the publisher is the copyright holder of this work and the author uses the Dutch legislation to make this work public.

Beamforming for a Fast Scanning Phased Array Weather Radar

Tworit Dash[#], Alexandru Gîrdianu[*#], Oleg A. Krasnov[#], Alexander G. Yarovoy[#]

[#]Microelectronics, TU Delft, The Netherlands

[*]NXP Semiconductors, Romania

{T.K.Dash, O.A.Krasnov, A.Yarovoy}@tudelft.nl, agirdianu@gmail.com

***Abstract* — At the airports, fast-scanning phased array radars are used to detect point-like targets, e.g., birds and drones. However, these radars do not possess Doppler processing and thus are not used for observation of the weather targets like precipitation events. A series of steps need to be performed, such as beamforming in elevation, target masking for weather-like targets, and Doppler processing to complete the signal processing chain for this kind of radar for weather-like targets. This paper focuses only on beamforming in elevation which is the first step in the direction of 3D wind field estimation for a fast-scanning phased array radar. The reiterative Minimum Mean Square Error (rMMSE) beamforming technique is proposed in this paper and has been used on real radar observations. The performance is analysed for the first time when noise is under or overestimated. The rMMSE beamformer has been compared with the Fourier (FR) and Capon (CP) beamformers.**

***Keywords* — fast scanning radars, phased array, Doppler velocity, target masks, beamforming**

I. Introduction

Detection of weather-like targets such as precipitation and estimation of wind velocity and direction, including turbulence intensity field, are vital tasks for airport radars. However, the existing radar technologies at the airports are well suited for detecting and tracking point-like targets such as birds and drones. The radars scan very fast in azimuth to have a fast update of the reflectivity profile in space. The faster the update, the better the tracking of the point-like targets. As only the reflectivity profile is needed in space, these radars do not perform any Doppler processing on the echoes in time. Range migration is one such popular technique used to resolve the dynamics of the point-like targets in the radar field of view [1] only with the reflectivity information. Due to the fast scanning nature, it limits the dwell time of the radar beam for a particular direction in space. The very short dwell time limits the radar performance as far as the Doppler processing is concerned. The radar that is discussed in this paper is the Max3D radar by Robin Radar [2]. It is a FCMW radar that scans the azimuth with a speed of $\Omega = 60$ rpm while on elevation it is electronically scanning in the interval 0° to 60°. In the processing chain, at first, beamforming is performed in the elevation using the re-iterative Minimum Mean Square Error "rMMSE" technique. It is compared with the classical beamforming techniques such as the Discrete Fourier Transform (FR) and Capon (CP) techniques. In addition to that, the paper presents the performance of the beamformers based on whether or not the noise information is under or overestimated. The performance of the beamformers is assessed with respect to sidelobe level reduction and Doppler moments estimation. This paper presents the verification of such beamforming techniques on real radar data with precipitation-like non-stationary distributed targets.

II. Radar parameters

Systems of antennas for MAX3D radar present two antennas for receiving, RX1 and RX2 and one for transmission, TX. The first receive antenna, RX1, called Main-Array, has 40 slotted waveguides lines, with a tilt angle of 15° and an electronic scanning interval $[0.5^\circ, 30^\circ]$, in the elevation. RX2 is called the Blind-spot-Array and has 8 elements, with a tilt angle of 45° and elevation interval $[30^\circ, 60^\circ]$. The thesis [3] can be followed for other details about the radar.

III. Beamforming

The beamforming is performed on the elevation axis represented as θ. Several beamforming techniques are applied with simulated data and also real radar data.

A. Signal Model

The array consists of M equally spaced identical antenna elements receiving l^{th} time sample of the complex radar return signal $\mathbf{x}_l$ ($\mathbf{x}_l$ is a vector of dimension $M \times 1$). The matrix $\mathbf{A}$ having a dimension of $(M \times K)$ consists of spatial steering vectors $\mathbf{a}(\theta)$. The vector $\mathbf{s}_l$ has a dimension of $(K \times 1)$, and it is associated with the complex radar return at an arbitrary range bin. A white Gaussian noise vector $\mathbf{n}_l$ is added with dimension $(M \times 1)$. As matrix $\mathbf{A}$ contains the steering vectors as a function of the antenna elements, the second dimension of $\mathbf{A}$, i.e., K, is the number of angular directions independent of the precipitation profiles. The vector $\mathbf{x}_l$ can be written as

$$\mathbf{x}_l = \mathbf{A}\mathbf{s}_l + \mathbf{n}_l \tag{1}$$

where

$$\begin{aligned} \mathbf{x}_l &= [x_{l,0}, x_{l,1}, \cdots, x_{l,M-1}]^T \\ \mathbf{s}_l &= [s_{l,0}, s_{l,1}, \cdots, s_{l,M-1}] \\ \mathbf{A} &= [\mathbf{a}(\theta_0)\mathbf{a}(\theta_1), \cdots, \mathbf{a}_{\theta_{K-1}}] \\ \mathbf{a}(\theta) &= [1 \ \exp(-j2\pi\Delta\sin(\theta)) \cdots \exp(-j2\pi(M-1)\Delta\sin(\theta))] \end{aligned} \tag{2}$$

Authorized licensed use limited to: TU Delft Library. Downloaded on November 07,2023 at 10:25:43 UTC from IEEE Xplore. Restrictions apply.

where $\Delta = \frac{d}{\lambda}$. Here, d is the distance between two consecutive antenna elements, and λ is the central wavelength of the radar. The operator $[\cdot]^T$ is the transpose of the matrix/ vector. The term j is the imaginary unit $\sqrt{-1}$. A beamformer tries to find filter weights such that the precipitation profile is as close as $\mathbf{s}_l$. If we consider the estimated weights are $\mathbf{w}_k$, then the estimated precipitation profile is given by

$$\hat{s}_{l,k} = \mathbf{w}_k^H \mathbf{x}_l \tag{3}$$

where $[\cdot]^H$ is the Hermitian operator.

B. Beamforming Techniques

The beamforming techniques that are studied for this radar are the Fourier, the Capon and the rMMSE algorithms. For details about how the Fourier and the Capon beamformers are applied, [3] can be followed. The rMMSE beamformer was first proposed in [4] for point-like targets. Later, this approach was extended for precipitation-like targets in [5]. The beamformer has the following expression.

$$\mathbf{w}_{MMSE_k} = \frac{\mathbf{R}^{-1}\mathbf{a}(\theta_k)}{\mathbf{a}^H(\theta_k)\mathbf{R}^{-1}\mathbf{a}(\theta_k)} \tag{4}$$

where $\mathbf{R}$ is the sample covariance matrix (SCM) and is given by

$$\mathbf{R} = \mathbf{A}\mathbf{R}_s\mathbf{A}^H + \mathbf{R}_n \tag{5}$$

The SCM has been decomposed into signal and noise covariances $\mathbf{R}_s$ and $\mathbf{R}_n$. The initialization of this beamformer is nothing but the Fourier beamformer. The steps of rMMSE are given as follows.

1) Prior information: The Fourier beamformer is used as the starting point for the rMMSE.

$$\hat{\mathbf{R}}_s^0 = \frac{1}{L}\hat{\mathbf{S}}_{FR}\hat{\mathbf{S}}_{FR}^H \odot \mathbf{I}_{K\times K} \tag{6}$$

where

$$\hat{\mathbf{S}}_{FR} = [\hat{\mathbf{s}}_0 \cdots \hat{\mathbf{s}}_{L-1}]$$
$$\hat{\mathbf{S}}_{FR} = \mathbf{W}_{FR}^H\mathbf{X}$$
$$\mathbf{W}_{FR} = [\mathbf{a}(\theta_0)\cdots\mathbf{a}(\theta_{K-1})]$$

2) Computation of the weight vectors: In each iteration i, the weights are updated using the updated covariance of the previous iteration.

$$\mathbf{w}_{MMSE_k}^{(i)} = \frac{\mathbf{R}^{(i)^{-1}}\mathbf{a}(\theta_k)}{\mathbf{a}^H(\theta_k)\mathbf{R}^{(i)^{-1}}\mathbf{a}(\theta_k)} \tag{7}$$

where

$$\mathbf{R}^{(i)} = \mathbf{A}\mathbf{R}_s^{(i)}\mathbf{A}^H + \mathbf{R}_n \tag{8}$$

3) Determination of rMMSE solutions: *K* new solutions are computed for each new set of weight vectors in order to update the space covariance matrix, $\mathbf{R}_s^{(i)}$.

$$\hat{\mathbf{S}}_{rMMSE}^{(i)} = \mathbf{W}_{rMMSE}^{(i)^H}\mathbf{X} \tag{9}$$
$$\mathbf{W}_{rMMSE}^{(i)} = [\mathbf{w}_{MMSE_0}^{(i)} \cdots \mathbf{w}_{MMSE_{K-1}}^{(i)}] \tag{10}$$

4) Reiteration: *i*+1 iterative space covariance matrix, $\hat{\mathbf{R}}_s$, calculated using *i*-iterative rMMSE solutions.

$$\hat{\mathbf{R}}_s^{i+1} = \frac{1}{L}\hat{\mathbf{S}}_{rMMSE}^{(i)}\hat{\mathbf{S}}_{rMMSE}^{(i)^H} \odot \mathbf{I}_{K\times K} \tag{11}$$

The algorithm jumps to step 2.

The algorithm stops when the minimum mean square error between two consecutive iterations

$$\delta_i = \frac{1}{N}\sum_{n=1}^{N}\left(\frac{\sum_{l=1}^{L}||\hat{\mathbf{s}}_{MMSE_{l,k}}^{(i)} - \hat{\mathbf{s}}_{MMSE_{l,k}}^{(i-1)}||^2}{\sum_{l=1}^{L}||\hat{\mathbf{s}}_{MMSE_{l,k}}^{(i-1)}||^2}\right) \tag{12}$$

reaches a threshold. The converged rMMSE is referred to as cMMSE henceforth.

IV. Results on Simulated Data

The performance of the rMMSE algorithm is assessed by sidelobes suppression and robustness to a limited number of Doppler bins. The analysis based on the abovementioned criteria is presented in detail in [5] for both point-like and extended targets. These results are reproduced in [3]. The targets considered in this simulation are extended targets. The radar signals are simulated by assuming that the Doppler velocity profiles for each target are Gaussian in nature [6]. From the analysis of simulated data in [3], the following is concluded.

1) FR accurately estimates the total power contained in the spectrum in the elevation ranges $[8.7°, 10.7°]$ and $[22.6°, 26.5°]$. The mean Doppler velocity and spectrum width estimated is closer to the true value where the total power is accurately estimated.
2) The FR technique shows little dependence on the number of Doppler bins. Here, the number of Doppler bins is considered at least 16.
3) The CP technique shows dependence on the number of Doppler bins.
4) Furthermore, it is observed that cMMSE(6) performances are superior as compared to the FR and CP techniques.

This paper also focuses on the algorithm performance in the case of underestimation or overestimation of noise variance, the parameter used to compute noise covariance matrix, $\mathbf{R}_n$. This study is not included in [5]. The input parameters for this case are listed in Table 1.

Table 1. Input parameters values for extended targets

	Extended Targets	
	LHS target	**RHS target**
Parameter	*Value*	*Value*
θ_{steer}	$[-0.5°$**to**$35°]$	
θ_{tg}	$10°$	$25°$
$\Delta\theta$	$0.97°$	
P	40 dB	60 dB
SNR	50 dB	
σ_n^2	10 dB	
$\sigma_{n_{M_0}}^2$	5.7 dB	
Doppler bins	16 and 256	
σ_D	1.5 m/s	

Authorized licensed use limited to: TU Delft Library. Downloaded on November 07,2023 at 10:25:43 UTC from IEEE Xplore. Restrictions apply.

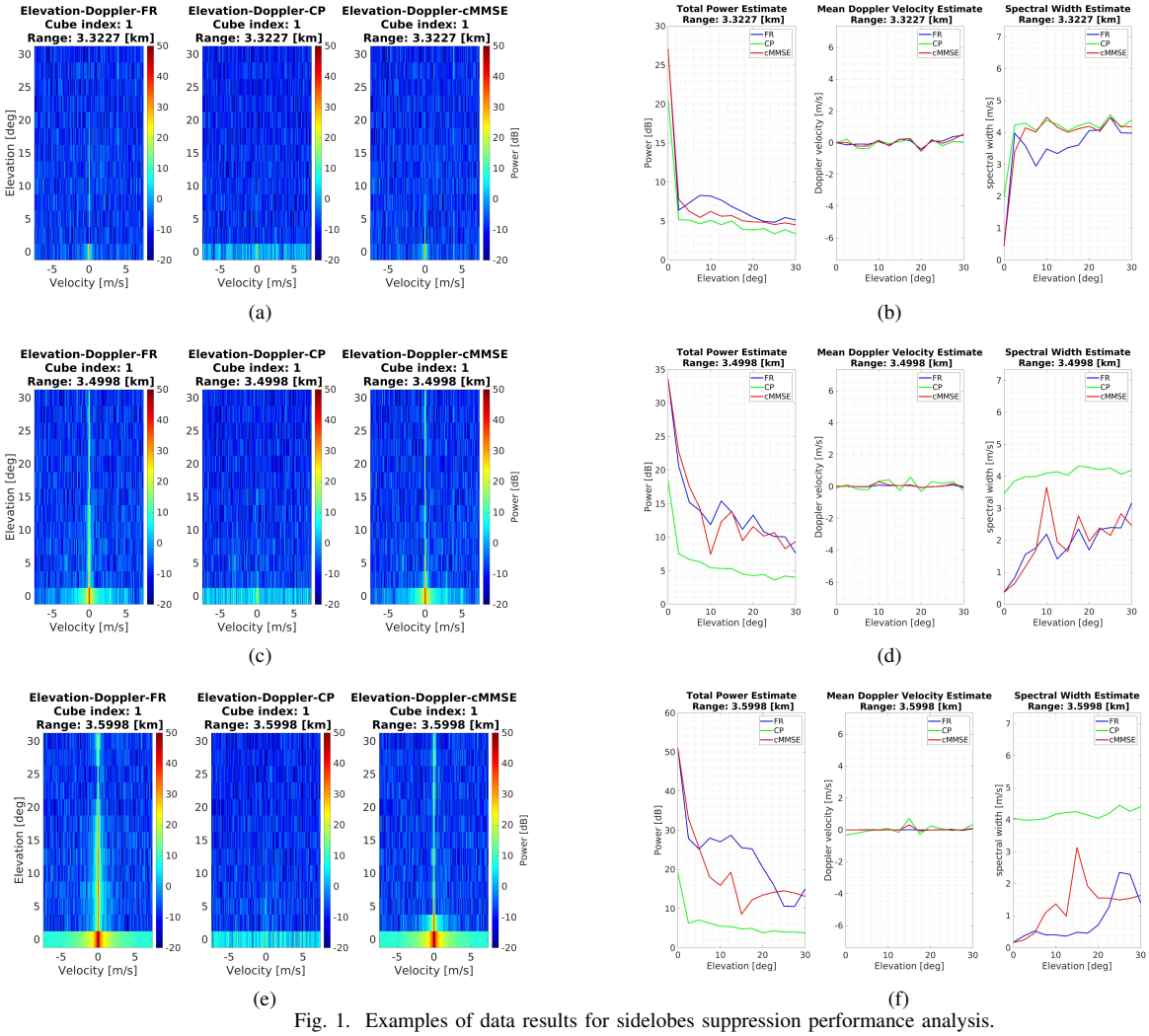

Fig. 1. Examples of data results for sidelobes suppression performance analysis.

Based on the results shown in Table 2, it can be concluded that the rMMSE provides better accuracy for the underestimation case than for the overestimation case. The necessary number of iterations differs in the over and under-estimation cases. Table 2 shows the performance of the rMMSE algorithm when the noise variance is over or underestimated. For overestimation, a noise variance of 20 dB, and for underestimation, a noise variance of 0 dB is used respectively. The true noise variance is 10 dB.

Table 2. Estimation accuracy for rMMSE when noise variance deviates from true value

	$\sigma_n^2 = 0$ **dB**		$\sigma_n^2 = 10$ **dB (true value)**		$\sigma_n^2 = 20$ **dB**	
Parameters	*mean bias*	*standard deviation*	*mean bias*	*standard deviation*	*mean bias*	*standard deviation*
total power dB	-1.8	3.5	-0.85	2.3	-0.99	2.75
mean Doppler velocity m/s	0.24	0.54	0.16	0.38	0.17	0.32
spectral width m/s	0.32	0.48	0.13	0.27	0.20	0.49
Number of iterations (i)	8		6		5	

V. Application to Real Radar Data

The real data is assessed by the following criteria.

1) Sidelobe level suppression: A specific range-azimuth cell is chosen where a ground target is present, and all the beamformers are assessed by elevation-Doppler maps.
2) Elevation-Doppler: The performance is analysed for all three beamformers on real data with a weather target using elevation-Doppler maps.

A. *Sidelobe level suppression*

The azimuth direction considered in the analysis is $\phi = 35°$. Substantial ground clutter is present at a range $r = 35$ km. Therefore, the elevation-Doppler map at this range-azimuth cell is analysed. In the following figure 1, the results are shown in increasing order of SNR. Every row corresponds to a single SNR. The first column for each SNR contains the 2D elevation-Doppler image plot with all three beamformers. The second column contains the Doppler moments (M_0 is the total power, M_1 is the mean Doppler velocity and M_2 is the Doppler spectrum width [7]) at each elevation with all

Authorized licensed use limited to: TU Delft Library. Downloaded on November 07,2023 at 10:25:43 UTC from IEEE Xplore. Restrictions apply.

three beamformers. The number of Doppler bins considered in this case is 256. Based on Fig. 1, it can be said that the CP method suppresses the sidelobes at 0° elevation even though it underestimates the total power. Based on the noise analysis performed in [3] for the same radar, it can be observed that the noise power at the same range is $\frac{\sigma_n^2}{M} = 8$ dB, where M is the number of antennas. Based on the relation between the noise floor and the noise power $\sigma_{n_{in}} = N\frac{\sigma_n^2}{M}dv$, ($N$ is the number of Doppler bins, dv is the velocity resolution), it can be said that the noise floor at this range-azimuth cell is $\sigma_{n_{in}} = 2.34$ dB for $N = 256$ and $dv = 0.0578$ m/s. The CP method, at higher elevations, reproduces this noise floor. Therefore, CP can be considered the benchmark in terms of sidelobe suppression. The cMMSE provides excellent sidelobe suppression at higher elevation angles and converges towards the CP results. It also provides a better estimation of the total power compared to FR and CP. However, in the second-row cMMSE does not suppress sidelobes and performs similarly to the FR. The estimation of M_1 remains constant in all the cases. The estimation of M_2, based on the CP benchmark, should converge to 4 m/s. However, it converges to this only on the first row. On the third row, at a higher elevation, cMMSE performs worse than the FR regarding sidelobe suppression.

B. Elevation Doppler Results

Fig. 2 shows results of elevation-Doppler for azimuth direction, $\phi = 35^\circ$, with a range within interval 10 to 11 km. The first row contains the elevation Doppler spectrum, and the second row includes the moments' estimation with all three beamformers. The cMMSE suppresses sidelobes around the target, but at higher elevation angles, the performance converges to the FR one. At higher elevation angles, the total power estimate of cMMSE is lower than that of the FR. Regarding spectral width, FR and cMMSE perform similarly, but within elevation interval 11° and 20°, cMMSE follows CP results, where FR oscillates around CP results.

VI. Conclusion

In this paper, the rMMSE beamformer is proposed for digital beamforming in the elevation plane and applied to the real radar data from the Max3D radar [2]. The beamformer performance is assessed alongside the Fourier and Capon beamformers. The beamformer has been applied on real radar observations with only clutter, and when distributed, non-stationary targets are present. The performance is analysed based on sidelobe level reduction and Doppler moments estimation. The rMMSE beamformer's performance is also studied when the noise variance is underestimated or overestimated. Regarding the suppression of sidelobes, the rMMSE algorithm performs better than the other two methods. The performance of CP is better than rMMSE at higher elevation angles. The performance of rMMSE converges to that of FR at higher elevation angles for specific cases of SNR. This research paves the way for the reconstruction of Doppler moments profiles in 3D in the future. With a multiple beam architecture in the elevation and mechanical scan over azimuth, all three spatial components of the true wind field can be estimated at each radar resolution volume.

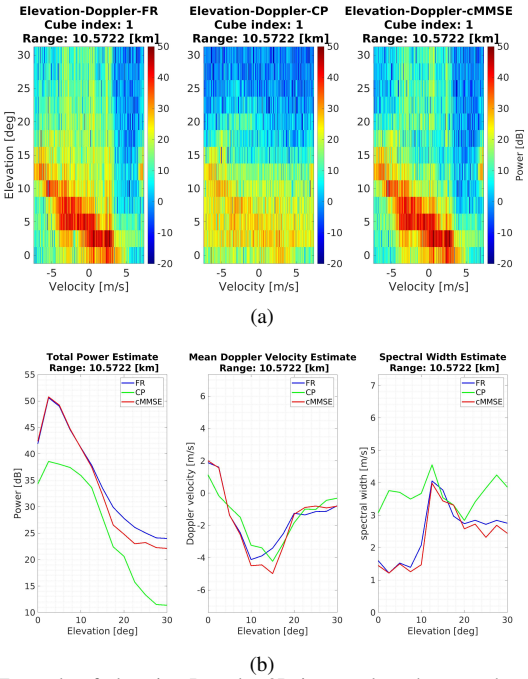

Fig. 2. Example of elevation-Doppler 2D image plot when weather target is present.

Acknowledgment

The authors are very grateful to our colleagues from Robin Radar Systems for their efforts and support in radar maintenance and data collection. This research was funded by the 'European Regional Development Fund (ERDF) via the Kansen voor West II program' under the project 'Airport Technology Lab'.

References

[1] J. M. Lopez-Sanchez and J. Fortuny-Guasch, "3-D radar imaging using range migration techniques," *IEEE Transactions on Antennas and Propagation*, vol. 48, no. 5, pp. 728–737, 2000.

[2] "Robin Radar Systems full 3D Advanced Bird Detection Radar - MAX3D." [Online]. Available: https://www.robinradar.com/max-avian-radar-system

[3] A. Gîrdianu, "Weather Targets Doppler Processing in Phased Array Radar with Fast Azimuthal Scanning," Tech. Rep., 2021.

[4] S. D. Blunt, T. Chan, and K. Gerlach, "Robust DOA estimation: The reiterative superresolution (RISR) algorithm," *IEEE Transactions on Aerospace and Electronic Systems*, vol. 47, no. 1, pp. 332–346, 2011.

[5] E. Yoshikawa, T. Ushio, Z. Kawasaki, S. Yoshida, T. Morimoto, F. Mizutani, and M. Wada, "MMSE beam forming on fast-scanning phased array weather radar," *IEEE Transactions on Geoscience and Remote Sensing*, vol. 51, no. 5, pp. 3077–3088, 2013.

[6] D. S. Zrnić, "Simulation of Weatherlike Doppler Spectra and Signals," *Journal of Applied Meteorology*, vol. 14, no. 4, 6 1975.

[7] T. Dash, O. A. Krasnov, and A. G. Yarovoy, "Performance Analysis of the Wind Field Estimation for a Very Fast Scanning Weather Radar," *Proceedings International Radar Symposium*, vol. 2022-Septe, pp. 420–425, 2022.

Authorized licensed use limited to: TU Delft Library. Downloaded on November 07,2023 at 10:25:43 UTC from IEEE Xplore. Restrictions apply.